International Journal of Nanoelectronics and Materials
IJNeaM
ISSN 1985-5761 | E-ISSN 2232-1535

Synthesis and Characterization of TiO_2 -CQDs Nanocomposites and Testing of Their Anticancer Potential

Maryam S. Jabbar [a] *, Olfat A. Mahmood [a], Zainab N. Jameel [b], and Noor. J. Jamal [b]

[a] *Department of Physics, College of Science, University of Diyala, Diyala 32011, Iraq.*
[b] *Communication Engineering Department, University of Technology- Iraq,10001 Baghdad, Iraq*
∗Corresponding author.Tel.: +9647903301734; fax: +964(1) 719-9644; e-mail:noor.j.jihad@uotechnology.edu.iq

Received 1 February 2023, Revised 8 May 2024, Accepted 16 July 2024

ABSTRACT

This work used a green approach to produce carbon quantum dots (CQDs). TiO_2 nanoparticles (NPs) and TiO2–CQDs nanocomposites with different weight ratios of CQDs were organized through a facile sol-gel method. XRD showed that the anatase and rutile phases of TiO_2 were polycrystalline with a tetragonal structure and that the CQDs exhibited a broad peak at (002) and a hexagonal structure. High resolution-transmission-electron microscopy revealed that the TiO_2 NPs agglomerated in mostly spherical shapes and that the anatase and rutile phases of TiO_2 had sizes of less than 15 and 25 nm, respectively. The CQDs had a relatively uniform diameter, a spherical shape with a highly crystalline structure, and a size below 2 nm. UV–visible spectroscopy revealed that the absorbance of the TiO_2- CQDs nanocomposites increased with the increase in CQD ratio. The energy band gaps of the anatase and rutile phases were 3.07 and 2.7 eV, respectively, whereas that of CQDs was 3.14 eV. Meanwhile, the energy band gaps of the TiO2–CQDs nanocomposites decreased with the increase in CQDs ratio. The growth inhibition rates of the liver cancer HepG2 cell line and the normal cell line RD were measured after 24 hours of experience to the two TiO_2 phases and TiO_2–CQDs nanocomposites. The cytotoxicity test presented that the tested substances were extremely harmful to cells in cancer. Inhibition rates increased with the increase in CQDs ratio. The inhibition rate of growth in cancer cells, including the liver cancer HepG2 cell line and the normal cell line (RD), was measured for 24 hours after they were exposed to TiO2 (two phases) and TiO2-CQDs nanocomposites. The samples showed a slight effect on the normal line (RD) compared to HepG2 cancer. The highest inhibition rate was 12.11% for the CQD 0.7 sample.

Keywords: *Anatase phase, Rutile phase, CQDs, HRTEM, Liver cancer.*

1. INTRODUCTION

In recent years, researchers have placed a notable emphasis on the study of nanoparticles (NPs) within the biomedical domain with a specific focus on their application in cancer treatment strategies.

NPs offer various advantages because they may quickly infiltrate tissues, bypass cellular barriers, and selectively localize and aggregate at tumor locations and can overcome rapid evacuation by the lymphatic system [1]. NPs can fulfill several functions because they can be concurrently employed for diagnostics and therapeutics determinations. The presence of light illumination can lead to the generation of reactive oxygen molecules (ROS) by metal or metal oxide NPs, resulting in the induction of cell death [2,3]. TiO_2 is a mineral that occurs naturally. It can be found in three distinct crystalline forms: anatase, rutile, and brookite. TiO_2 NPs have emerged as a novel category of inorganic chemical compounds that have found extensive applications in numerous fields, including cosmetics, pollution remediation, food preservation, medicines, and painting [4,5]. In recent times, TiO_2 has been applied in the field of biomaterials [6, 7, 8]. TiO_2 NPs have been utilized as a photodynamic treatment agent for different cancer cell types, including HepG2, a human cell line used to treat hepatocellular carcinoma, K592, leukemia, cervical cancer, MCF7 and MDA-MB-468 breast epithelial cells, and no small cell lung cancer are among the human cell lines used in these studies [9–13]. The sol–gel method is a widely utilized technique for producing TiO_2 NPs due to its comfort of usage, cost effectiveness, and high success rate. It provides a means for synthesizing TiO_2NPs have many morphologies, including wires, rods, sheets, tubes, particles, mesoporous structures, and aerogels [14].
A previous study extensively investigated carbon quantum dots (CQDs), a type of carbon NPs [15]. CQDs have particle sizes of 10 nm or less. By contrast, graphene nanosheets have planar sizes of less than 100 nm and are referred to as graphene quantum dots [16]. CQDs possess attributes, such as chemical inertness, biocompatibility, low toxicity, and cost-effectiveness, that are distinct from those of well-known quantum dots with semiconducting properties; akin to semiconductor quantum dots, they also demonstrate enhanced fluorescence [17]. The hydrothermal method is a suitable synthetic technique for the synthesis of CQDs with precise control over their size. It allows for the production of CQDs with highly regulated

sizes from different organic compounds and carbohydrates [18,19]. Biocompatibility and nontoxicity are essential properties that determine the suitability of CQDs for several biomedical techniques, particularly in the area of cancer treatment. These properties are crucial prerequisites for the successful utilization of CQDs in novel approaches aimed at combating cancer. Some works have investigated the biotoxic effects of CQD on various cancer cells, such as HepG2 [20], Hek 293 [21], and A549 [22].

Furthermore, certain green-synthesized CQDs have demonstrated exceptional fluorescence characteristics as well as notable bioactivities, including antioxidizing, anticancer, and anti-inflammatory capabilities. A previous work investigated the strong inhibition of cancer cells by photoluminescent CQDs derived from green tea [23]. Another work employed a different method for creating fluorescent CQDs from chitosan derivatives and investigated their biodistribution, cytotoxicity, and antioxidant properties [24]. Furthermore, scholars have researched the potential of aspirin-derived carbon dots as biocompatible materials for bioimaging purposes while also exhibiting anti-inflammatory properties [25,26].

Here, we present the integration of the up conversion of TiO_2 and CQD microspheres by using a straightforward sol–gel technique. The in vitro cytotoxicity of the resulting compounds was assessed by investigating their effects on the HepG2 cell line, which is derived from human liver cancer, and the RD normal cell line, which represents normal liver tissue.

2. EXPERIMENTAL DETAILS

2.1 Synthesis of TiO_2 NP Powder Via the Sol–Gel Method

The initial materials consisted of $TiCl_4$ with a purity of 99.99% and ethanol (CH_3CH_2OH) with a purity of 99.99%. Synthesis was completed by introducing a series of droplets derived from $TiCl_4$ into an absolute ethanol solution at a ratio of 1:10. The reaction was conducted under a chemical fume hood with the help of a magnetic stirrer to remove unwanted toxic gases, such as cloud HCl, while the temperature was maintained at room temperature. The above synthesis procedure yielded a pale-yellow solution with pH values of 1.4–2. The gel state was successfully obtained after subjecting the obtained solution to a temperature of 80 °C for 12 h. The anatase phase was obtained through calcination at 450 °C for 1.5 h. By contrast, the rutile phase was obtained through calcination at 900 °C for 1.5 h.

2.2 Synthesis of CQDs Via a Green Method

CQDs were prepared through hydrothermal carbonization, which involves mixing ethanol with natural raw materials and carbonizing the mixture at relatively low temperatures. The primary processes involved in hydrothermal carbonization are the dehydration, polymerization, and carbonization of tiny nonconjugated molecules. These molecules, which are commonly present in orange juice, include citric acid, glucose, sucrose, fructose, and ascorbic acid. Production of CQD is the process's final result. To create a yellow solution, the necessary amount of ethanol was mixed with the right amount of pulp-free orange juice in a mixer. The solution-containing glass dish was put inside a stainless-steel autoclave and sealed tight. The autoclave's interior had an atmosphere of one atmosphere pressure and was set at a temperature of around 120 degrees Celsius. The process was completed within approximately 150 min. The autoclave was switched off and allowed to gradually cool to room temperature after the prescribed amount of time had elapsed. Subsequently, 40 mI of the resulting dark brown solution was extracted. The solution underwent centrifugation and additional washing with dichloromethane and a ~~a~~ significant amount of acetone to create a liquid phase and deposit, which were then separated. The deposit had dried. The powder that formed from the dried deposit was considered as CQDs. TiO_2 NPs and X-ray diffraction, UV-Vis-NIR spectrophotometry, and high-resolution transmission electron microscopy (HRTEM) were used to analyze CQDs.

2.3 Synthesis of TiO2–CQD Nanocomposites

TiO_2–CQD nanocomposites were synthesized by using the sol–gel method. Two combinations of composites were prepared by mixing 0.3 g of TiO_2 (anatase phase) and various quantities of CQDs (0.3 and 0.7 × 100% [w/w]). Each mixture was put to 20 mI of deionized water, agitated for three hours, and then dried for twelve hours at 80 °C in an oven. A UV-Vis spectrophotometer was used to evaluate the samples.

2.4 Anticancer Activity

The preservation and care of cell cultures were performed as follows: The HepG2 cancer cell line and RD normal cell line was cultured together in a culture container with a surface area of 25 cm^2. 10% calf B serum were added to RBMI-1640, the culture medium. The cell suspension and culture medium were placed in containers and incubated in a 5% CO_2 incubator at 37 °C for 24 h.

2.4.1 Cytotoxicity assays

Cells for the determination of the cytotoxic effect of the two TiO2 phases and TiO2–CQD nanocomposites were prepared by treating the contents of a 25 cm^2 tissue culture container with trypsin/versine solution. The cells were then incubated in an incubator at 37 °C for 10 min and added with 20 mI of culture medium supplemented with serum. The cell suspensions were mixed well0.2 mL of the resultant mixture was then cautiously added to each well of a tissue culture plate with a flat bottom. For 24 hours, the plate was incubated at 37 °C. Subsequently, the previous culture medium was discarded, and 0.2 mI of the pre-prepared extract was added at different concentrations to the wells, with three replicates for each concentration. Three additional replicates were created. Control plates, which consisted only of the cell suspension, were incubated at 37 °C. After 24 h of exposure, the plates were removed from the incubator, and a crystal violet staining solution was added to all wells containing cells at a rate of 100 µI per hole. The plates were returned to the

incubator for 20 min and then removed. ELISA results were read at a wavelength of 492 nm. The following formula was used to determine the percentage of cytotoxicity, or the inhibition rate of cell growth. [21]:

Inhibition rate = (A – B) /A × 100 .....(1)

where A is the control group's optical density and B is the optical density of the samples that are being studied.

2.4.2 Statistical analysis

The statistical evaluation of the results was conducted by using Graph Pad Prism Version 6 analysis software and analysis of variance. Means were compared by using the Duncan multiplex experiment, wherein significant differences were observed at a probability threshold of $P < 0.05$.

3. RESULTS and DISCUSSIONS

3.1 X-ray Diffractions Analysis

X-ray diffractions analyses was conducted to determine the structure and phases of TiO2 NPs. Figure 1(a) displays practically the crystal types in the spectrum acquired at 450 °C. The intensity peaks indicate that the anatase phase had a polycrystalline nature and a tetragonal structure oriented at the 2θ diffraction angles of 25.52°, 37.04°, 38.01°, 38.67°, 48.23°, 54.09°, 55.26°, 62.87°, 68.95°, 70.43°, and 75.25° that corresponded to the diffraction planes of (101), (103), (004), (112), (200), (105), (211), (204), (116), (220), and (215), respectively. These findings are in line with the International Center for Diffraction Data (ICDD) card number 21-1272 and comparable to those reported by other studies [27,28]. The same figure depicts that at 900 °C, the rutile phase had polycrystalline TiO2 peaks and a tetragonal structure oriented at the 2θ diffraction angles of 27.55°, 36.17°, 39.31°, 41.33°, 44.14°, 54.41°, 56.72°, 62.82°, 64.14°, 69.10°, 69.88°, and 76.40° that corresponded to the diffraction planes of (110), (101), (200), (111), (210), (211), (220), (002), (310), (301), (112), and (202), respectively. These findings are in line with the ICDD card numbers 21-1276 and comparable to those reported by other researchers [27]. The increase in temperature led to the agglomeration of particles and the transformation of the TiO2 phase from anatase to rutile, resulting in an elevation in the intensity of X-ray diffraction. Furthermore, as crystallite size increased, the diffraction peaks exhibited a profile that was narrower than that of the TiO2 calcite at 900 °C. The XRD pattern in Figure 1(b) of the CQDs shows a broad peak at 19.42°, which corresponded to the (002) hkl plane with hexagonal structure. This result is in agreement with the ICDD card number 48-1206 and comparable to those reported by other studies [29,30].

In this investigation, Scherrer's formula was utilized to determine crystallite size [28]:

$$D = 0.9\,\lambda / (\beta \cos\theta) \quad \ldots\ldots\ldots\ldots \quad (2)$$

where the symbol *D* represents the crystallite sizes, λ denotes the X-ray wavelengths associated with the CuKα line emission, β represents the full width at half maximum, and θ signifies Bragg's angle. Calculations showed that the crystallite sizes of the anatase and rutile phases were 15.89 and 40.54 nm, respectively. The crystallite size of CQDs was 1.28 nm.

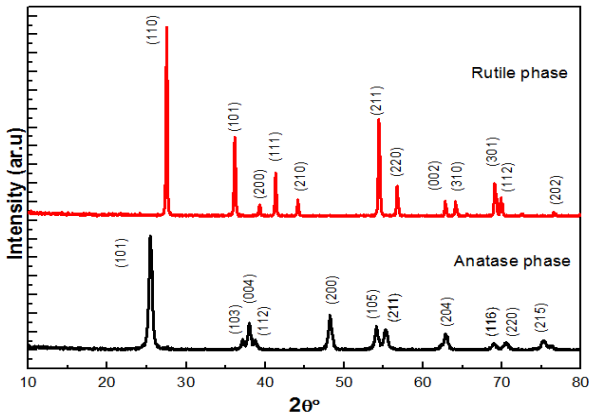

Figure.1 (a) **X**-ray diffraction patterns of TiO2 NPs.

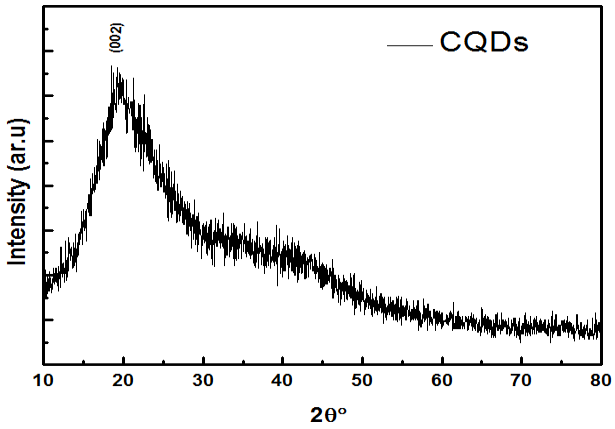

Figure.1 (b) X-ray diffraction patterns of CQDs .

3.2 High resolution transmission electron microscopy

HRTEM was conducted to examine the microstructure of the prepared materials. The HRTEM images of TiO2 NPs and CQDs are displayed in Figures 2 and 3, respectively. Figure 2(a) displays that the TiO2 NPs (anatase phase) agglomerated in a mostly spherical form and that their dimensions was less than 15 nm. When the preparation temperature increased, the anatase phase turned into the rutile phase, the size of the granules increased, and the granules grew in different forms with sizes of less than 25 nm, as shown in Figure 2(c). This result supports and is consistent with our XRD data on particle size. This consistency can be attributed to the correlation between the increase in temperature and the subsequent rise in atomic kinetic energy. As a result, atoms are likely to accept their appropriate places within the crystal lattice, thus contributing to the enlargement of grain size [31]. Figures 2(b) and 2(d) illustrate that the lattice spacing of the anatase and rutile phases was almost 0.31 nm.The HRTEM descriptions of the CQDs are provided in Figures 3(a) and 3(b). Figure 3(a) shows that the CQDs had a relatively uniform, dot-like spherical shape with a highly crystalline structure and a size of less than 2 nm. These results support and are consistent with our XRD data on particle size. Figure 3(b) reveals that CQDs' lattice spacing

was 0.24 nm. The photoluminescence (UCPL) feature of the material [32]. These results are consistent with those of previous studies[33].

300–400 nm. Beyond this particular region, the correlation gradually declined with the increase in wavelength, as visually depicted in Figure4(b). The absorbance of TiO_2–CQD nanocomposites increased with the increase in CQD ratio due to the upconversion

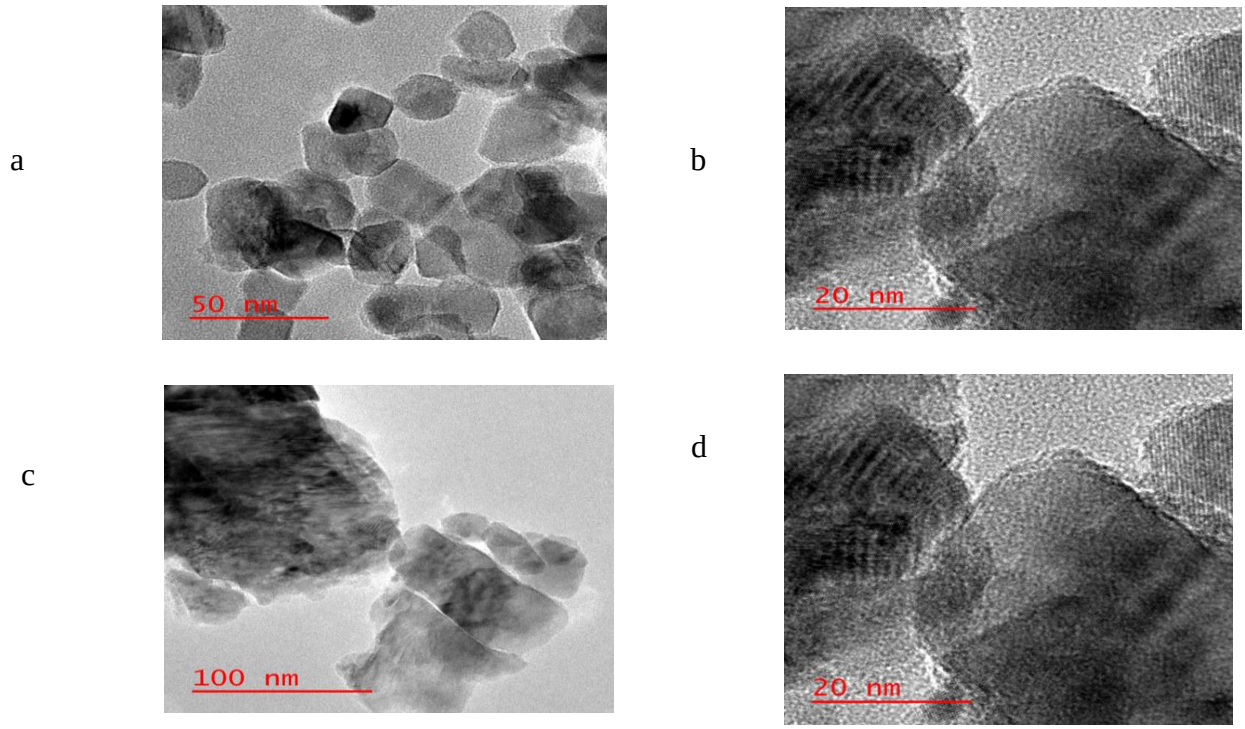

Figure. 2 HRTEM images of TiO2 NPs .

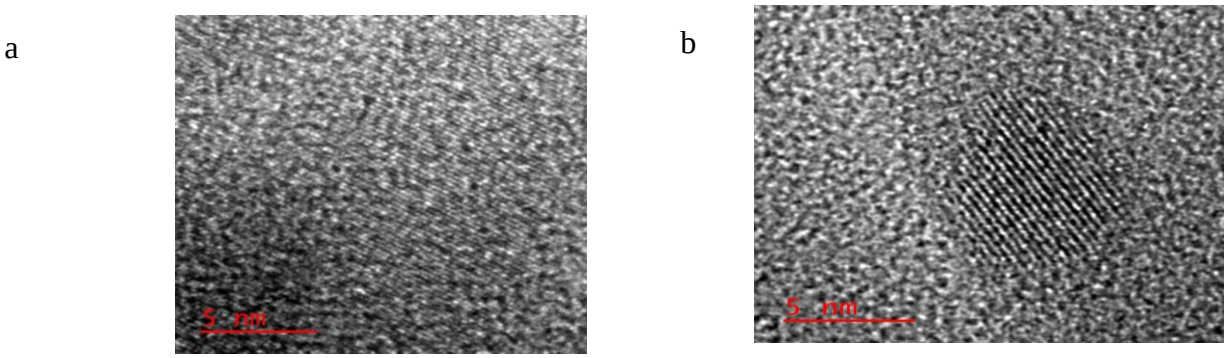

Fig. 3 HRTEM images of CQDs .

3.3 Optical Studies

UV-Vis and NIR absorbance spectra obtained spanning the wavelength range of 300900 nm were used to evaluate the optical properties of the manufactured materials. Figure 4 shows the absorbance spectra of CQDs, TiO_2NPs, and TiO_2-CQD nanocomposites as a function of wavelength. The absorption of the two TiO_2 phases decreased gradually with an increase in wavelength. However, as shown in Figure (4a), the absorption of TiO2 in the anatase phase was lower than that of TiO_2 in the rutile phase; this result is consistent with a previously reported finding [34]. Figure 4(b) illustrates that the absorbance of CQDs decreased slowly with the increase in wavelength (300–900 nm). The absorbance of the TiO_2–CQD nanocomposite exhibited a rapid decrease in the wavelength region of

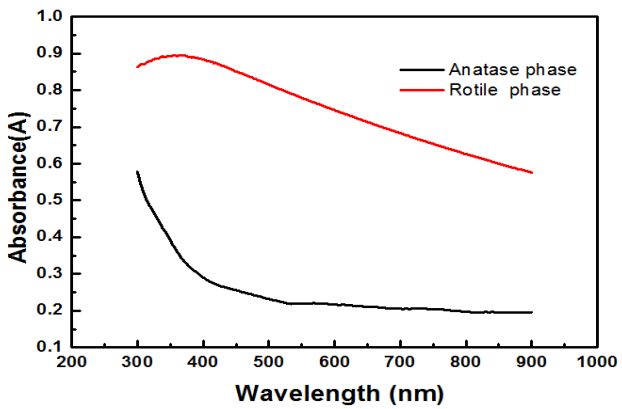

Figure.4 (a) Absorption spectra of TiO_2 Np anatase and rutile phases.

Tauc's equation was utilized to ascertain the values of the optical energy gap (Eg), which may be stated as follows[32]:

$$h\upsilon = B_o(h\upsilon - E_g^{opt})^r \quad \ldots\ldots(3)$$

where hν denotes the photon energy, and *B* denotes a constant that lacks reliance on photon energy and r. Figure 5 presents the plot of $(\alpha h\upsilon)^2$ versus hυ, and Eg values were calculated by using Tauc's equation.

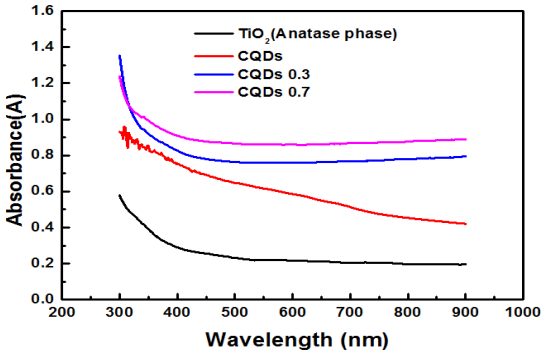

Figure. 4(b) Absorption spectra of TiO_2, CQDs, and TiO2–CQDs nanocomopsites.

Figure 5(a) shows that the energy band gaps of the anatase and rutile phases were 3.07 and 2.7 eV, respectively, which agreed with the reported values [32]. As displayed in Figure 5(b), the energy band gap of CQDs was 3.14 eV, which was consistent with previously reported results [35,36]. The Eg values of the TiO_2-CQD nanocomposites decreased with increasing CQD ratio. As shown in Figure 5(c), CQD 0.3 and CQD 0.7 had energy band gaps of 2.88 and 2.26 eV, respectively, which were in agreement with previously reported results [33]. These results suggested that because of CQDs' small band gap and upconversion, modification might significantly increase TiO_2's capacity to absorb visible light. This modification technique was different from carbon element doping, which forms a new energy level in the band gap of TiO_2 by inserting carbon atoms into the interface and surface lattice. This process results in visible light absorption. [33].

3.4 Anticancer study

Two cell lines, namely, the cancer cell line HepG2 and normal cell line RD, were exposed to TiO_2 phases and TiO_2–CQD nanocomposites at a concentration of 100 µg/m for 24 h in an incubator at 37 °C. Figures 6 and 7 show that these substances killed the tested cells, and Table (1) shows that the TiO_2 NPs and TiO_2–CQD nanocomposites had an inhibitory impact on the growth of the HepG2 and RD cell lines for 24 h after exposure. Initially, the cytotoxicity effects of the two TiO_2 phases were tested. The results provided in the table below reveal that the anatase phase had a higher rate of inhibition of HepG2 and RD cell lines than the rutile phase because the anatase phase is smaller than the rutile phase, as demonstrated by XRD and HRTEM measurements. As their size decreased, the surface area of the materials increased. Therefore, the nanomaterials became able to agglomerate, and lateral dispersion increased. These effects increased the interactions of the nanomaterials with cells and their absorption by cells, leasing to the programmed death of the HepG2 and RD cell lines [37]. Given that the anatase phase had the best inhibitory effect on cells, it was chosen for the preparation of TiO_2–CQD nanocomposites. The results presented that the inhibition rate of the HepG2 cell line increased with increasing CQD concentration. The percentage of inhibition by sample CQD 0.7 reached 81.01%. The inhibition rate of the normal line RD was lower than that of the HepG2 cancer line. The percentage of inhibition by sample CQD 0.7 reached 12.11%, as shown in ~~the~~ Table 1. This result indicated that the prepared nanomaterials did not affect healthy cells. Because CQDs have advantageous qualities such high water solubility, biocompatibility, and dispersibility, the percentage of inhibition by TiO_2-CQD nanocomposites rose with increasing CQDs ratio. Furthermore, CQDs can narrow semiconductor materials' band gaps, which boosts the production of ROS [38,39].

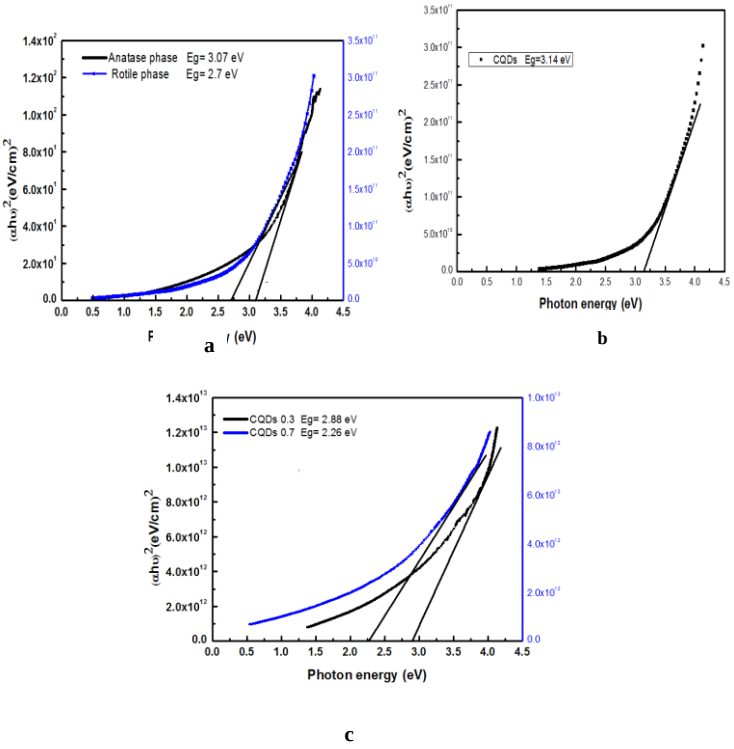

Figure. 5 Tauc plots of TiO2 (a), CQDs (b), and TiO2–CQDs nanocomposites (c).

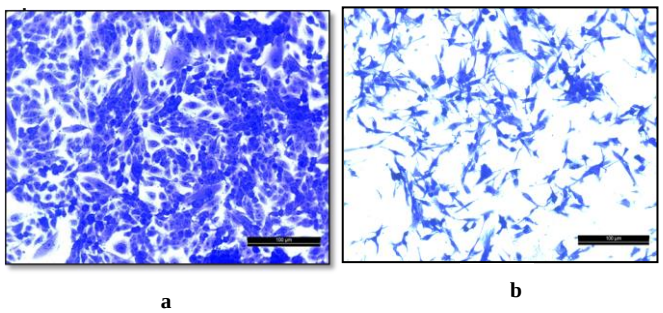

Figure. 6 Comparison of the HepG2 cell lines under treatment with TiO_2–CQD nanocomposites (a), the control (b), and TiO_2–CQD nanocomposites with a CQD ratio of 0.7.

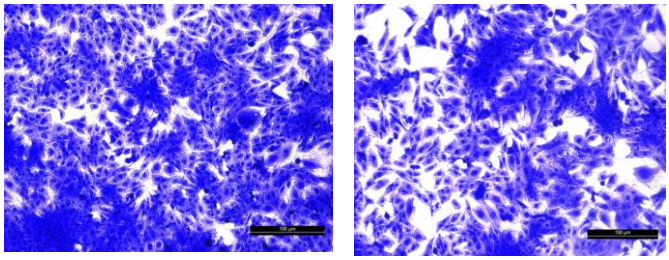

a b

Figure. 7 Comparison of the RD cell lines under treatment with TiO_2–CQDs nanocomposites (a), the control, and (b) TiO_2–CQDs nanocomposites with a CQDs ratio of 0.7.

Table 1. Inhibitory effect of TiO_2 NPs and TiO2–CQDs nanocomposites on the cancer cell line HepG2 and normal cell line RD.

Inhibition ratio of cancer cell line HepG2		**Inhibition ratio of normal cell line (RD)**	
Samples	**Inhibition Ratio100%**	**Samples**	**Inhibition Ratio100%**
anatase phase	67.42	**anatase phase**	5.13
rutile phase	35.19	**rutile phases**	1.08
CQDs 0.3	71.39	**CQDs 0.3**	6.23
CQDs 0.7	81.01	**CQDs 0.7**	12.11

4. CONCLUSION

Studying the operational, morphological, as well as optical characteristics of the prepared materials revealed that the anatase and rutile phases of TiO_2 were polycrystalline with a tetragonal structure and that CQDs exhibited a broad peak at (002) and hexagonal structure. The HRTEM results indicated that the sizes of the anatase and rutile phases of TiO2 were less than 15 and 25 nm, respectively, and that of CQDs was less than 2 nm. The results of UV–Vis spectroscopy presented that the absorbance of the TiO_2–CQDs nanocomposites increased with the increase in CQDs ratio. The Eg values of the TiO_2–CQDs nanocomposites decreased with the increase in CQDs ratio. TiO_2 and the TiO_2–CQDs nanocomposites were highly cytotoxic against the HepG2 and RD cell lines, and the rate of cytotoxicity increased with the increase in CQDs ratio. This result indicated that the prepared materials have promising uses against cancer cells.

ACKNOWLEDGMENTS

The authors would like to thank the Engineering College and the Department of Physics at the University of Diyala College of Science for providing the chance to work on this article.

REFERENCES

[1] B. Elvin, H.Shen, and M. Ferrari. "Principles of nanoparticle design for overcoming biological barriers to drug delivery." Nature biotechnology 33.9 ,941-951, 2015.

[2] D. man, F. Demir, et al. "Enhanced photodynamic therapy and fluorescence imaging using gold nanorods for porphyrin delivery in a novel in vitro squamous cell carcinoma 3D model." Journal of Materials Chemistry B 8.23 ,5131-5142,2020.

[3] W. Shizhong, et al. "Nanomaterials and singlet oxygen photosensitizers: potential applications in photodynamic therapy." Journal of Materials Chemistry 14.4 ,487-493,2004.

[4] Chen X., and S. Mao. "Titanium dioxide nanomaterials: synthesis, properties, modifications, and applications." Chemical reviews 107.7, 2891-2959,2007.

[5] C. Y. Jin, B. S. Zhu, X. F. Wang and Q. H. Lu, "Cytotoxicity of Titanium Dioxide Nanoparticles in Mouse Fibroblast Cells," Chemical Research in Toxicology, Vol. 21, No. 9, 2008.

[6] R. Chacon, D M et al. "Fibronectin and vitronectin promote human fetal osteoblast cell attachment and proliferation on nanoporous titanium surfaces." Journal of biomedical nanotechnology vol. 9,6 ,1092-7 ,2013.

[7] C. López de Dicastillo, M. Guerrero Correa, F. B. Martínez, C. Streitt, and M. José Galotto, "Antimicrobial Effect of Titanium Dioxide Nanoparticles", Antimicrobial Resistance - A One Health Perspective. IntechOpen, Mar. 03, 2021.

[8] G.Ang et al. "The effects of titania nanotubes with embedded silver oxide nanoparticles on bacteria and osteoblasts." Biomaterials vol. 35,13 ,2014.

[9] Sh. Hongyuan et al. "Enhancement of the photokilling effect of TiO2 in photodynamic therapy by conjugating with reduced graphene oxide and its mechanism exploration." Journal of photochemistry and photobiology. B, Biology vol. 177 , 112-123. ,2017.

[10] M. Mohammad Amin et al. "Photodynamic N-TiO2 Nanoparticle Treatment Induces Controlled ROS-mediated Autophagy and Terminal Differentiation of Leukemia Cells." Scientific reports, vol. 6 34413. 4 Oct. 2016.

[11] L. Zheng et al. "Comparison of the killing effects between nitrogen-doped and pure TiO2 on HeLa cells with visible light irradiation." Nanoscale research letters ,vol. 8,1 96. 22 Feb. 2013.

[12] L. Nefeli et al. "Effect of nanostructured TiO_2 crystal phase on photoinduced apoptosis of breast cancer epithelial cells." International journal of nanomedicine vol. 9 3219-30. 3 Jul. 2014 .

[13] W. Yurong et al. "Cytotoxicity, DNA damage, and apoptosis induced by titanium dioxide nanoparticles in human non-small cell lung cancer A549 cells." Environmental science and pollution research international vol. 22,7 ,2015.

[14] Z. Miao, et al. "Electrochemically induced sol–gel preparation of single- crystalline TiO2 nanowires." Nano Letters, **2**, pp. 717-720,2002.

[15] Zh.Ran et al. "Recent advances in carbon dots: synthesis and applications in bone tissue engineering." Nanoscale vol. 15,7 3106-3119. 16 Feb., 2023

[16] D. Yongqiang et al. “Graphene quantum dots, graphene oxide, carbon quantum dots and graphite nanocrystals in coals.” Nanoscale vol. 6,13 ,2014.

[17] L. Shi Ying et al. “Carbon quantum dots and their applications.” Chemical Society reviews vol. 44,1 ,2015.

[18] B. Ali et al. “Synthesis of biocompatible and highly photoluminescent nitrogen doped carbon dots from lime: analytical applications and optimization using response surface methodology.” Materials science & engineering. C, Materials for biological applications vol. 47 ,2015.

[19] Y. A. Mahmood and B. T. Chiad, “Synthesis and spectroscopic study of highly fluorescent carbon dots derived from orange juice with Stilbene 420 dye”, IJP, vol. 18, no. 44, pp. 62–68, Mar. 2020.

[20] W. Zhu Lian et al. “A general quantitative pH sensor developed with dicyandiamide N-doped high quantum yield graphene quantum dots.” Nanoscale vol. 6,7 ,2014.

[21] P. Eepsita et al. “Comparative In Vitro Cytotoxicity Study of Carbon Dot-Based Organometallic Nanoconjugates: Exploration of Their Cell Proliferation, Uptake, and Localization in Cancerous and Normal Cells.” Oxidative medicine and cellular longevity vol. 2022 3483073. 15 Mar. 2022 .

[22] W. Zhu Lian et al. “One-pot hydrothermal synthesis of highly luminescent nitrogen-doped amphoteric carbon dots for bioimaging from Bombyx mori silk - natural proteins.” Journal of materials chemistry. B vol. 1,22 ,2013.

[23] H.Pin-Che et al. “Extremely high inhibition activity of photoluminescent carbon nanodots toward cancer cells.” Journal of materials chemistry. B vol. 1,13 ,2013.

[24] L. Dongmei et al. “Fluorescent Carbon Dots Derived from Maillard Reaction Products: Their Properties, Biodistribution, Cytotoxicity, and Antioxidant Activity.” Journal of agricultural and food chemistry vol. 66,6 ,2018.

[25] X. Xiaowei et al. “Aspirin-Based Carbon Dots, a Good Biocompatibility of Material Applied for Bioimaging and Anti-Inflammation.” ACS applied materials & interfaces vol. 8,2016.

[26] Z. Shaojing et al. “Green Synthesis of Bifunctional Fluorescent Carbon Dots from Garlic for Cellular Imaging and Free Radical Scavenging.” ACS applied materials & interfaces vol. 7,31 ,2015.

[27] S. Abel et al. “Biosynthesis of TiO2 nanoparticles by Caricaceae (Papaya) shell extracts for antifungal application.C Scientific reports vol. 12,1 15960. 24 Sep. 2022.

[28] L. KS, et al. Biological approach to synthesize TiO2 nanoparticles using Staphylococcus aureus for antibacterial and antibiofilm applications. J Microbiol Exp ;8(1):36-43, 2020.

[29] H. Yang, et al. Valorization of expired passion fruit shell by hydrothermal conversion into Carbon Quantum Dot: physical and optical propertie“,Waste and Biomass Valorization. 12,pp. 2109-2117,2021.

[30] Sh. Asiya F ,et al. “Bioinspired Carbon Quantum Dots: An Antibiofilm Agents.” Journal of nanoscience and nanotechnology vol. 19,4 ,2019.

[31] W. Daranfed et al. “ temperature influence on ZnS thin films prepared by ultrasonic spray", Thin Solid Films, vol.518 pp. (1082-1084),2009.

[32] S. Hamdan, “photodetector based on rutile and anatase TiO2 nanostructures/n-Si heterojunction", Journal of Physics: Conference Series. vol.2114 pp. 1-9,2021.

[33] K. Jun et al. “Upconversion carbon quantum dots as visible light responsive component for efficient enhancement of photocatalytic performance.” Journal of colloid and interface science vol. 496 ,2017,

[34] Jihad, Noor J., and Murooj A. Abd Almuhsan. "Enhancement on the performance of Radio-over-Fiber ROF technology." Journal of Optics 53, no. 2 , 1447-1455,2024.

[35] U.Remli, “Photocatalytic degradation of methyl orange using Carbon Quantum Dots (CQDs) derived from watermelon rinds.” Materials Science and Engineering. vol.736 pp.1-6,2020.

[36] A. H Abd, “ASynthesis of Carbon Quantum Dot by electro-chemical method and studying optical, electrical, and structural properties.”, Chemical Methodologies,vol. 6 .pp. 823-830,2022.

[37] Jabbar, Maryam S., et al. "Synthesis and photocatalytic applications of TiO2-CQDs nanocomposites prepared by biological methods." Baghdad Science Journal ,2024.

[38] Yan, Y., Kuang, W., Shi, L., Ye, X., Yang, Y., Xie, X., Shi, Q., Tan, S. (2019) Carbon quantum dot-decorated TiO2 for fast and sustainable antibacterial properties under visible-light, Journal of Alloys and Compounds, vol.777 pp. 234-243,2010.

[39] Jameel, Z.N., Jihad, N.J. “The imperfections of the screen to camera OCC systems. ”,J Opt 53, 3743–3748 (2024). https://doi.org/10.1007/s12596-023-01512-3.